I&EC research
Industrial & Engineering Chemistry Research

Article

pubs.acs.org/IECR

Direct Simulations of Mixing of Liquids with Density and Viscosity Differences

J. J. Derksen*

Chemical & Materials Engineering, University of Alberta, Edmonton, Alberta, T6G 2G6 Canada

ABSTRACT: Simulations of flow and scalar transport in stirred tanks operated in transitional and mildly turbulent regimes (Re = 3000−12000) are presented. The moderate Reynolds numbers allow the flow to be simulated directly, without the use of turbulence closure or subgrid-scale models. The Newtonian liquids that are blended have different densities and/or viscosities, and the emphasis is on how these differences affect mixing times. The density difference is characterized by a Richardson number (Ri) that varies in the range of 0−0.5. The kinematic viscosity ratio is between 1 and 4. The results show that mixing times increase steeply with increasing Ri and that changing the tank layout can partly mitigate this effect. The viscosity ratio has a much weaker influence on the mixing time.

INTRODUCTION

Mixing of miscible liquids (i.e., blending) is a basic operation in many food, pharmaceutical, and chemical processes. For batch processes, mixing is usually carried out in stirred tanks. The time to homogenization (mixing time) is a key process characteristic that depends on the geometry of the mixing device (impeller and tank layout), the operating conditions (such as impeller speed), and the liquids involved in the process. If the liquids involved all have the same uniform mechanical properties (i.e., they all have the same density and viscosity and are Newtonian), the dimensionless mixing time (e.g., represented by a number of impeller revolutions until a certain predefined level of homogeneity is reached) depends on the geometry as defined in geometrical aspect ratios and the Reynolds number (and possibly the Froude number if the tank has a free surface). Uniformity of the mechanical properties of the tank's contents before the blending process is completed, however, is not a common situation; the liquids to be blended usually have different viscosities and/or densities. It is expected that the density and viscosity differences have consequences for the flow structures in the tank and, therefore, for the mixing time.

With nonuniform contents in the agitated tank, the number of (nondimensional) parameters characterizing the mixing process quickly grows: Not only do multiple densities and viscosities enter the parameter space, but the initial conditions and/or the way in which the various liquid components are added to the tank also come into play. Investigating mixing times over the entire parameter space and for all blending scenarios is obviously impossible. It is the intent of this article to focus on the consequences of density and viscosity differences on mixing times for a limited number of situations involving two different liquids that are initially completely segregated and each occupy roughly one-half of the tank volume. The latter implies that the mechanical properties of both liquids determine the overall flow in the tank; as an example, we do not consider small additions of liquid A in a large pool of liquid B. In the latter situation, the properties of one liquid (i.e., B) likely dominate the mixing process.

The specific systems that are considered are conceptually simple. The two miscible liquids are placed in a mixing tank with the interface between them at half of the tank height. If the two liquids have different densities, the light liquid occupies the upper part of the volume, and the heavy liquid occupies the lower part. Until time zero, this fully segregated system has zero velocity everywhere. Then, at time zero, the impeller is switched on to a constant angular velocity, and the blending process is monitored. The impeller used throughout this research is a pitched-blade turbine with four blades under an angle of 45°; the tank is cylindrical and has a flat bottom and four equally spaced baffles along its perimeter. In a recent article of ours,[1] the above scenario was executed to assess the effect of density differences on mixing time. The scope of the present article is much broader than that of ref 1 in that, now, viscosity differences and also different stirred-tank layouts are considered, in addition to density differences.

The research described here is purely computational with an interest in *turbulent* mixing. As is well-known, for simulations of strongly turbulent flows, turbulence modeling is required; direct simulation of the flow is generally not an option because of the broad spectrum of length scales involved[2] that would all need to be resolved. In turbulence modeling, parametrizations for the smaller length scales are applied (as in large-eddy simulation),[3] or the statistics of the fluctuations present in the flow are modeled and taken into account in the (ensemble- or time-averaged) equations of fluid motion (Reynolds averaging).[4] Single-phase, turbulent flow in complex geometries such as agitated tanks is a clear challenge for turbulence models.[5−9] This is because the localized energy input (the stirrer) induces very strong inhomogeneity and anisotropy and keeps the turbulence away from a dynamic equilibrium state. To this complexity, we now add a liquid composition field that varies in space and time, with the viscosity and density being a function

Received: January 5, 2012
Revised: April 3, 2012
Accepted: April 22, 2012
Published: April 23, 2012

dx.doi.org/10.1021/ie3000419 | *Ind. Eng. Chem. Res.* 2012, 51, 6948−6957

of the local, time-dependent composition. Because our focus is on the effects of the local viscosity and density on the mixing process, we do not want our results to be (potentially) corrupted by the way turbulence models deal with these localized effects. For this reason, we do not apply turbulence modeling in our simulations. The price to pay is that we are limited to relatively modest Reynolds numbers (in this work, the default value is Re = 6000 with some excursions toward 12000, where Re is precisely defined below), so that we (at least) strive for direct resolution of the flow. The choice for direct simulations requires a study of the effects of grid resolution on the flow field and on the mixing time results.

This article is organized in the following manner: First, the flow system is described, dimensionless numbers are defined, and the parameter ranges covered in this research are identified. Subsequently, the simulation procedure is outlined schematically with references to the literature for further details. We then present results. The emphasis is on the effect of a density difference on the mixing time and on ways to mitigate the prohibitively long mixing times encountered in some cases by changing the impeller location and/or direction of rotation. Because liquids with different densities often also have different viscosities, flow with local viscosity variation was studied as well. The impact of grid resolution is discussed in a separate subsection. Conclusions are summarized in the last section.

FLOW SYSTEMS

The tank and agitator and the coordinate system used in this work are shown in Figure 1. The tank is cylindrical, with four

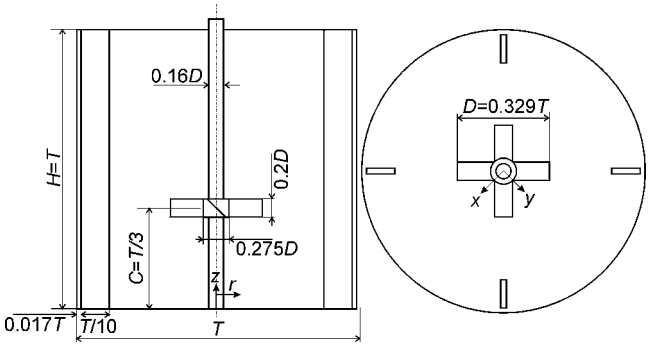

Figure 1. Stirred-tank geometry considered: a baffled tank with a pitched-blade impeller. The coordinate systems [(r,z) and (x,y,z)] are fixed and have their origin at the center of the bottom of the tank. The top of the tank is closed off with a lid. In addition to an impeller-to-bottom distance of $C = T/3$ (as shown in the figure), a distance of $C = T/2$ was considered as well. The impeller can rotate both ways, so that it can pump downward (default) and upward.

equally spaced baffles along its perimeter. The flow is driven by four pitched (45°) blades attached to a hub that is mounted on a shaft that runs over the entire height of the tank. The tank is closed off with a lid so that, at the top surface (as on all other solid surfaces), no-slip conditions apply. The Reynolds number of this flow system is defined as $Re = (ND^2/\overline{\nu})$, where N is the impeller speed (in revolutions per second), D is the impeller diameter (see Figure 1), and $\overline{\nu}$ is the tank-volume-averaged kinematic viscosity. Figure 1 shows the geometry with the impeller placed at a distance of $C = T/3$ above the flat tank bottom. We studied the consequences of changing the off-bottom clearance by also performing simulations for $C = T/2$. The impeller was operated in both down-pumping and up-pumping modes.

Initially, two layers of liquid are placed in the tank, with their interface at $z = 0.5H$. The upper liquid has a density that is $\Delta\rho$ less than that of the lower liquid; that is, the system starts from a stable stratification. The denser liquid has either the same kinematic viscosity as the lighter liquid or a higher viscosity ($\nu_D \geq \nu_L$, where ν_D and ν_L are the viscosities of the dense and light liquids, respectively). Starting from a completely still situation, we switch on the impeller with constant speed of N.

In addition to the Reynolds number, a Richardson number defined as $Ri = (g\Delta\rho/\overline{\rho}N^2D)$ and the kinematic viscosity ratio $Vi \equiv \nu_D/\nu_L$ fully pin down the flow system. In the expression for Ri, g is gravitational acceleration, and $\overline{\rho}$ is the volume-averaged density of the liquid in the tank. Rielly and Pandit[10] defined the Richardson number as $g\Delta\rho H/\rho N^2D$). Given the (standard) aspect ratios used in the present work, the latter expression is equal to 3 times the Richardson number as defined herein.

The default Reynolds number used was 6000. Systems with Re = 3000 and 12000 were simulated as well. Specifically, for the latter value, resolution effects need to be carefully assessed. This Reynolds number range covers transitional and mildly turbulent flow—at least for single-liquid systems. The Richardson number ranged from 0.0 to 0.5, and the viscosity ratio from 1.0 to 4.0. The latter are moderate viscosity ratios, so that very thin striations of the highly viscous phase in the less viscous phase[11] are not to be expected. As for the higher Reynolds number, the impact of spatial resolution on the blending process was assessed for the highest viscosity ratio, Vi = 4.0.

MODELING APPROACH

The lattice-Boltzmann method (LBM) was applied to numerically solve the incompressible flow equations.[12,13] The method originates from the lattice-gas automaton concept as conceived by Frisch, Hasslacher, and Pomeau in 1986.[14] Lattice gases and lattice-Boltzmann fluids can be viewed as collections of (fictitious) fluid particles moving over a regular lattice and interacting with one another at lattice sites. These interactions (collisions) give rise to viscous behavior of the fluid, just as collisions/interactions among molecules do in real fluids. The main reasons for employing the LBM for fluid flow simulations are its computational efficiency and its inherent parallelism, both not being hampered by geometrical complexity.

In this article, the LBM formulation of Somers[15] is employed. It falls in the category of three-dimensional, 18-speed (D3Q18) models. Its grid is uniform and cubic. Planar, no-slip walls naturally follow when bounce-back conditions are applied. For nonplanar and/or moving walls (which we have because we are simulating the flow in a cylindrical, baffled mixing tank with a revolving impeller), an adaptive force field technique (i.e., an immersed boundary method) has been used.[16,17]

The local composition of the liquid is represented by a scalar field c (with c = 1 representing pure light fluid and c = 0 representing pure dense fluid) for which we solve the transport equation

$$\frac{\partial c}{\partial t} + u_i\frac{\partial c}{\partial x_i} = \Gamma\frac{\partial^2 c}{\partial x_i^2} \qquad (1)$$

(with summation over repeated indices) where u_i is the ith component of the fluid velocity vector and Γ is a diffusion

dx.doi.org/10.1021/ie3000419 | Ind. Eng. Chem. Res. 2012, 51, 6948−6957

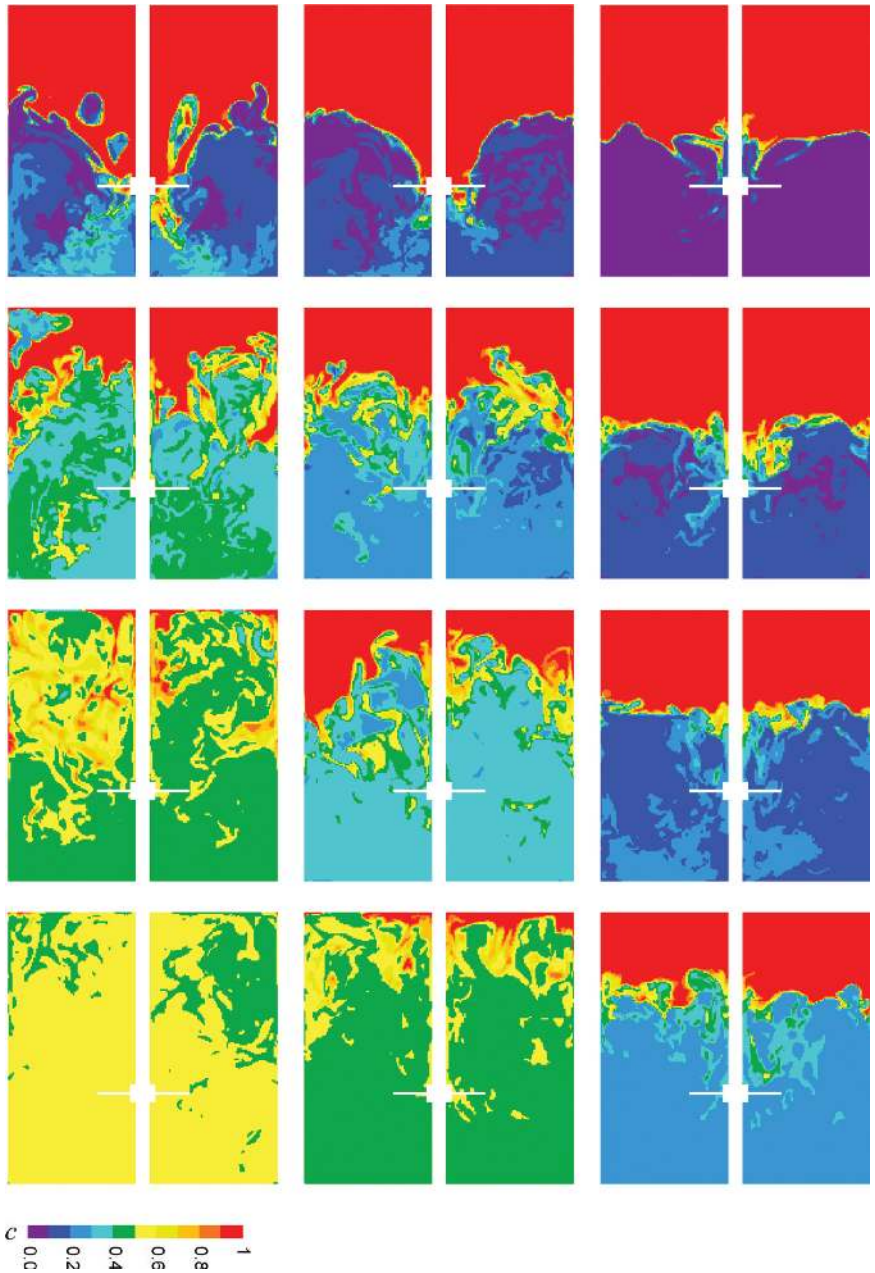

Figure 2. Liquid composition c in a vertical, midbaffle plane at (from top to bottom) 10, 20, 30, and 50 impeller revolutions after startup. From left to right, Ri = 0.0, 0.125, and 0.5. All cases: Re = 6000 and Vi = 1.0. Down-pumping impeller at clearance $C = T/3$.

coefficient that follows from setting the Schmidt number, $Sc \equiv \nu/\Gamma$, equal to 1000. We solve eq 1 with an explicit finite-volume discretization on the same (uniform and cubic) grid as the LBM. A clear advantage of employing a finite-volume formulation is the availability of methods for suppressing numerical diffusion. As in previous works,[18,19] total-variation-diminishing (TVD) discretization with the Superbee flux limiter for the convective fluxes[20] was employed. We step in time according to an Euler explicit scheme. This explicit finite-volume formulation for scalar transport does not hamper the parallelism of the overall numerical approach.

Strictly speaking, the Schmidt number is the fourth dimensionless number (next to Re, Ri, and Vi) defining the flow. Its large value (10^3) makes the micro-scalar scale (Batchelor scale) a factor of $(Sc)^{1/2} \approx 30$ smaller than the Kolmogorov length scale and quite impossible to resolve in our numerical simulations. In the simulations—although we suppress numerical diffusion as much as possible—diffusion is controlled by the grid spacing, and the precise value of Sc based on molecular diffusivity has a marginal impact on the computational results. To assess the extent to which numerical diffusion influences the outcomes of our simulations, grid effects were assessed, as discussed later in the article.

The scalar concentration field c is two-way-coupled to the flow field; that is, c is convected by the flow (see u_i in eq 1), and at the same time, it affects the flow because c determines the local viscosity and density of the liquid mixture. For viscosity as well as density, linear dependencies in c are assumed: $\nu_{mx} = \nu_D - c(\nu_D - \nu_L)$ and $\rho_{mx} = \overline{\rho} + ({}^1/_2 - c)\Delta\rho$, where ν_{mx} and ρ_{mx} are the local mixture viscosity and density, respectively. The lattice-Boltzmann method is able to directly deal with the place- and time-varying viscosity. The density is incorporated through a

dx.doi.org/10.1021/ie3000419 | Ind. Eng. Chem. Res. 2012, 51, 6948−6957

Boussinesq approximation: A liquid element having density ρ_{mx} feels a body force in the positive z direction (as defined in Figure 1) of $f_z = g(\bar{\rho} - \rho_{mx}) = g\Delta\rho(c - {}^1/_2)$, and this force is incorporated into the LB scheme. In the Boussinesq approximation, the body force term is the only place where the density variation enters the Navier–Stokes equations. For this approximation to be valid, it must be true that $\Delta\rho/\bar{\rho} \ll 1$ [that is, $Ri \ll g/(N^2D)$].

Numerical Settings. The default grid (which, as explained above, is uniform and cubic) has a spacing Δ such that 180Δ corresponds to the tank diameter T. The number of time steps to complete one impeller revolution is 2000. As a result, the tip speed of the impeller is $\pi ND = 0.094$ in lattice units (with an impeller diameter of $D = T/3$), which keeps the flow velocities in the tank well below the speed of sound of the lattice-Boltzmann system, thus achieving incompressible flow. To assess grid effects (related to the flow as well to scalar transport), a number of simulations were performed on finer grids: $T = 240\Delta$, 330Δ, 420Δ, and 552Δ. Because of the explicit nature of the lattice-Boltzmann method and its (in)compressibility constraints, the finer grids required more time steps per impeller revolution (up to 6400 for the finest grid).

The microscale of turbulence (Kolmogorov length scale η) relates to a macroscopic length scale (say, the tank diameter T) according to $\eta = T \times Re^{-3/4}$. The criterion for sufficiently resolved direct numerical simulations of turbulence is $\Delta < \pi\eta$.[21,22] According to this criterion, at $Re = 6000$, a grid with $T = 180\Delta$ slightly under-resolves the flow; at our highest Reynolds number ($Re = 12000$), the same grid has $\Delta \approx 6.4\eta$, and the finest grid (with $T = 552\Delta$) has $\Delta \approx 2.1\eta$. As discussed above, full resolution of the Batchelor scale (η_B) is not an option, as it is a factor of 30 smaller than the Kolmogorov scale, so that, on the finest grid and at $Re = 12000$, $\Delta \approx 60\eta_B$. The consequences of not resolving η_B were assessed through grid refinement.

The relatively modest default resolution of $T = 180\Delta$ was chosen to limit computational cost and, at the same time, to allow for a significant number of simulations with sometimes long time spans (up to 300 impeller revolutions) required to reach sufficient levels of homogeneity so that mixing times could be determined. The large number of cases is the result of parameter variations: Re, Ri, Vi, off-bottom impeller clearance, and direction of rotation of the impeller were all varied.

RESULTS

Flow and Scalar Field Impressions for a Down-Pumping Impeller at $C = T/3$. The results of our simulations are discussed mostly in terms of the flow and concentration fields in the vertical, midbaffle cross section as they evolve in time from startup from a zero-flow, fully segregated, stable state. The set of base cases that begins this section focuses on the effect of a density difference (and thus of Ri) on mixing. It has $Re = 6000$, $Vi = 1.0$, and an impeller at $C = T/3$ that pumps the liquid downward. Figure 2 shows the scalar concentration fields for three different values of Ri and at different moments after startup of the impeller. One of cases is nonbuoyant and thus a passive-scalar case ($Ri = 0.0$ and $Vi = 1.0$). Buoyancy clearly impacts the mixing process. At $Ri = 0.0$, the interface between high and low concentration quickly disintegrates, and low-concentration blobs appear in the high-concentration upper portion of the cross section as a result of three-dimensional flow effects, largely because of the presence of baffles. At $Ri = 0.125$, this is less the case. The interface is clearly agitated but largely maintains its integrity (i.e., it is not broken up). At still larger Ri ($Ri = 0.5$ in Figure 2), the interface stays more or less horizontal. It rises as a result of erosion: High-concentration (and thus low-density) liquid is eroded from the interface and drawn down to the impeller. It then quickly mixes in the lower part of the tank. This leads to a gradual rise of concentration in the part of the tank underneath the interface. The portion above the interface stays at the initial concentration and gradually reduces in height. The interface also acts as a barrier for momentum transfer: Above the interface, there is hardly any flow, and the flow that is there is mainly generated by the revolving shaft that extends into that region, not so much by the action of the impeller (see Figure 3, which has a logarithmic color scale).

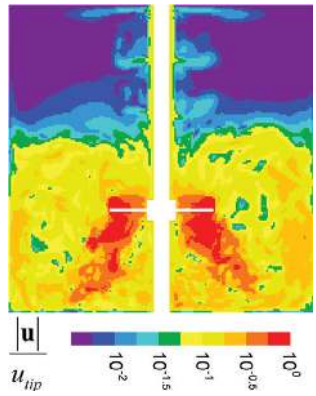

Figure 3. Instantaneous realization 50 revolutions after startup of the velocity magnitude in a midbaffle plane for $Ri = 0.5$, $Vi = 1.0$, and $Re = 6000$ and a down-pumping impeller at $C = T/3$. Note the logarithmic color scale.

Compared to the impact of the Richardson number, the effect of the Reynolds number is relatively modest, as can be assessed from Figure 4, in which we compare, at $Ri = 0.125$ and $Vi = 1.0$, the scalar concentration fields in the midbaffle plane at $Re = 3000$ and $Re = 12000$ at two moments in time. These fields have their $Re = 6000$ counterparts displayed in Figure 2 (middle column, second and fourth panels from the top). At all three Reynolds numbers, the interface reaches a level of $z \approx 2.2D$ after 20 revolutions and is close under the lid after 50 revolutions.

A viscosity ratio larger than 1 has an interesting effect on the mixing process: See Figure 5, where results for the highest viscosity ratio ($Vi = 4.0$) are shown. Because the upper liquid is now less viscous, it is easier for momentum to penetrate the upper parts of the tank volume; the interface between dense and light liquids gets more agitated compared to corresponding situations for $Vi = 1.0$ (see Figure 2). At the same time, the higher viscosity in the lower part of the tank slows homogenization there (again compare Figure 5 with corresponding panels of Figure 2). The net result of these opposing effects on mixing time is assessed in the next section.

Mixing Time Analysis. Mixing times were analyzed based on the scalar concentration fields in the midbaffle, vertical cross sections through the tank. In these cross sections, we monitored the spatial concentration standard deviation as a function of time

dx.doi.org/10.1021/ie3000419 | Ind. Eng. Chem. Res. 2012, 51, 6948–6957

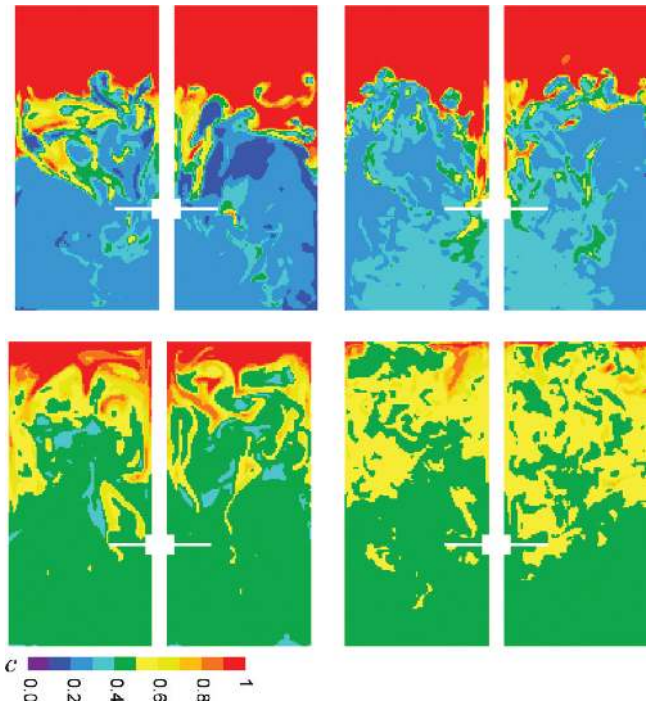

Figure 4. Assessment of Reynolds number effects at Ri = 0.125 and Vi = 1.0 for a down-pumping impeller at $C = T/3$. (Left) Re = 3000, (right) Re = 12000. (Top) 20 and (bottom) 50 impeller revolutions after startup.

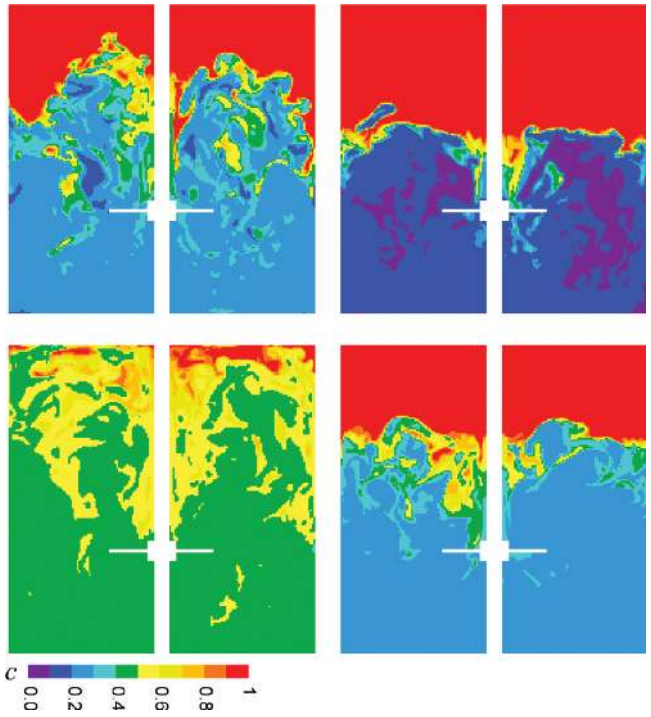

Figure 5. Assessment of viscosity ratio effects at Re = 6000 with a down-pumping impeller at $C = T/3$. (Left) Ri = 0.125, Vi = 4.0; (right) Ri = 0.5, Vi = 4.0. (Top) 20 and (bottom) 50 impeller revolutions after startup. Compare with the corresponding panels in Figure 2 for Vi = 1.0.

$$\sigma^2(t) = \frac{1}{A}\iint_A \{c^2(x, y = 0, z, t) - [\langle c\rangle(t)]^2\}\mathrm{d}x\mathrm{d}z$$

where $\langle c\rangle(t)$ is the average scalar concentration in the midbaffle plane at moment t. At time zero, the liquids are fully segregated, with c = 1 in the upper half of the cross section, c = 0 in the lower half, and $\langle c\rangle$ = 0.5, so that the starting value of the standard deviation is $\sigma(t = 0)$ = 0.5.

For a down-pumping impeller at clearance $C = T/3$, the time series of standard deviations are given in Figure 6 for Re = 6000, Vi = 1.0, and various Richardson numbers. The decay rates strongly depend on the Richardson number; at Ri = 0.03125 the scalar variance decay is close to that of a passive scalar, so one can conclude that (for the specific stirred-tank configuration and process conditions) buoyancy influences the homogenization process if $Ri \geq 0.0625$. To characterize the decay of scalar variance with a single number, the time to reach σ = 0.025 was chosen here as the mixing time measure τ_σ. Figure 7 shows how the dimensionless mixing time $\tau_\sigma N$ depends on Ri and Re for Vi = 1.0.

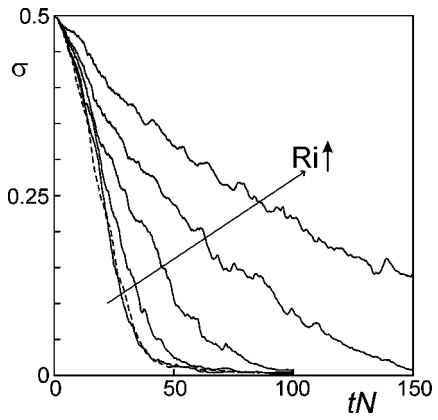

Figure 6. Scalar standard deviation in the midbaffle plane (σ) as a function of time; comparison of different Richardson numbers for a down-pumping impeller at clearance $C = T/3$, Re = 6000, and Vi = 1.0. The dashed curve has Ri = 0.0. The solid curves have Ri = 0.03125, 0.0625, 0.125, 0.25, and 0.5 in the order indicated.

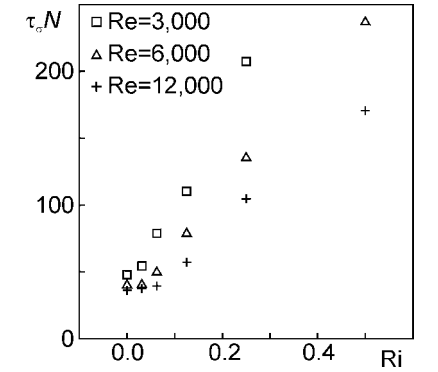

Figure 7. Mixing time based on scalar standard deviation (τ_σ) versus Ri at three different Reynolds numbers. Down-pumping impeller at $C = T/3$, Vi = 1.0.

As discussed in our previous article,[1] for Ri = 0.0 and Vi = 1.0 (i.e., no buoyancy and no viscosity variation), the above-defined measure τ_σ agrees with correlations for mixing times (symbol τ_M) based on experimental data: Grenville et al.[23] suggested $\tau_M N = 5.1(Po)^{-1/3}(T/D)^2$, where Po is the power number [which is the power P drawn by the impeller made

dx.doi.org/10.1021/ie3000419 | Ind. Eng. Chem. Res. 2012, 51, 6948−6957

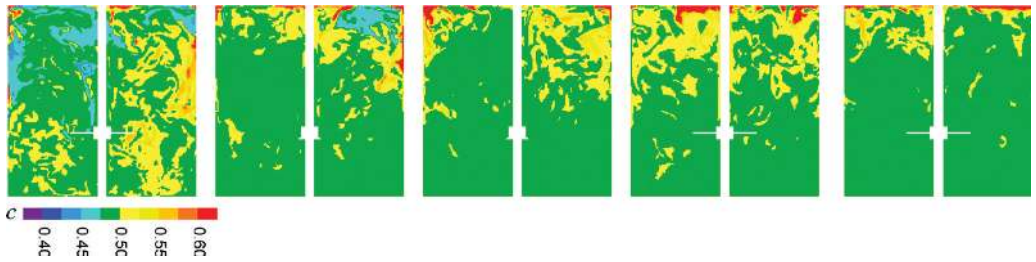

Figure 8. Concentration fields in the midbaffle plane the moment just after the $\sigma = 0.025$ level was reached for the cases shown in Figure 6 (except the $Ri = 0$ case). From left to right: $Ri = 0.03125$, 0.0625, 0.125, 0.25, and 0.5. Note that the color scaling is finer than in Figures 2 and 4.

dimensionless according to $Po \equiv P/(\rho D^5 N^3)$]. The mixing time data in Figure 7 for $Ri = 0.0$ are $\tau_\sigma N = 47.8$, 40.1, and 36.1 for $Re = 3000$, 6000, and 12000, respectively. For a four-blade, 45° down-pumping pitched-blade turbine with $C = T/3$ and $T/D = 3$, Chapple et al.[24] reported Po in the range of 1.1−1.2 for $10^3 \leq Re \leq 10^4$. The power numbers derived from our simulations are slightly higher: $Po = 1.37$, 1.35, and 1.34 for $Re = 3000$, 6000, and 12000, respectively. The mixing time correlation then gives $\tau_M N$ in the range of 41−44, which is close to the results for $\tau_\sigma N$ presented in Figure 7 for $Ri = 0.0$ and $Vi = 1.0$. To some extent, this agreement justifies our choice for taking $\sigma = 0.025$ as the uniformity criterion.

Summarizing the mixing process in the single number $\tau_\sigma N$ is a strong simplification, however. In Figure 8, the concentration fields at a moment just after the level $\sigma = 0.025$ has been reached are given for the simulations of Figure 6 with nonzero Ri. Note that, in this figure, the color scale is enhanced to emphasize deviations from the (ultimate) $c = 0.5$ concentration. The states of mixing for the different Richardson numbers are clearly different, although $\sigma \approx 0.025$ in all cases. For high Ri, the concentration throughout the tank is fairly uniform except for a few patches with high c near the lid. For lower Ri, there is more (though weaker) variation in c throughout the tank. Despite these observations, in the following discussion, the results of our simulations are summarized mainly in terms of $\tau_\sigma N$.

Figure 7 shows how, in the case of uniform kinematic viscosity ($Vi = 1.0$), the dimensionless mixing time $\tau_\sigma N$ relates to Ri and Re: the higher Ri, the larger the mixing time; the larger Re, the lower the mixing time. Buoyancy amplifies the differences in mixing times between the various Reynolds numbers: At $Ri = 0.0$, the mixing times of the three Reynolds numbers are within 25%. By $Ri = 0.0625$, this has grown to some 50%, and differences increase further for higher Ri. Specifically, homogenization at the lowest Reynolds number (3000) slows dramatically. At this Re value, the stratification makes it hard to sustain turbulence, specifically in the higher levels of the tank. Reduced fluctuation levels also have a negative impact on the interface erosion process that, as discussed above, becomes increasingly rate-determining at higher Richardson numbers.

The viscosity ratio affects the mixing time only weakly; see Figure 9. If there is any discernible trend in this figure, it is a slight increase in mixing time with Vi. As demonstrated in the discussion of the effects of spatial resolution later in this article, however, the differences in Figure 9 are of the same order of magnitude as the differences between different grids and are therefore considered not to be significant.

Impeller Rotational Direction and Off-Bottom Clearance. As is clear from Figure 7, the mixing time is a strong function of the Richardson number, with much longer mixing times for higher Ri values. This is sufficient reason to investigate

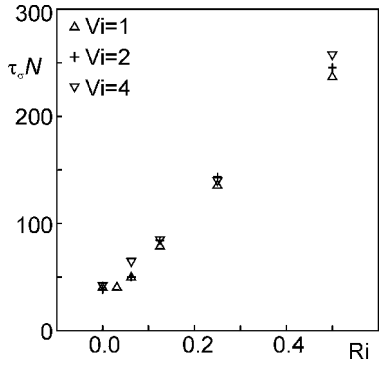

Figure 9. Mixing time based on scalar standard deviation (τ_σ) versus Ri at three different viscosity ratios. Down-pumping impeller at $C = T/3$, $Re = 6000$.

whether simple/minor design changes can accelerate the blending process. As a first simple change, the rotation direction of the impeller was reversed so that it pumped liquid upward (i.e., in the direction against gravity). This implies that the denser liquid was directly pumped into the upper part of the tank that contained lighter liquid. It also implies that the interface between light and dense liquid became much more agitated. The consequences for the mixing process for a relatively high Richardson number of 0.5 ($Re = 6000$ and $Vi = 1.0$) can be observed in Figure 10 (left panels). Reversing the impeller helped in dramatically decreasing the mixing time as compared to that obtained with the down-pumping impeller (see Figure 11, left panel). For $Ri \geq 0.125$ a reduction of $\tau_\sigma N$ by a factor of 2 or more was achieved. As can be seen in Figure 10 (lower left panel), in the final stages of mixing, a layer of light liquid persisted in the top part of the tank that became rate-limiting for the mixing process.

As a possible solution, we considered placing the (still) up-pumping impeller higher in the tank at $C = T/2$. This indeed removed the lighter liquid from the top of the tank more quickly but instead left denser liquid at the bottom (middle panels of Figure 10). In terms of dimensionless mixing time, the up-pumping impeller at $C = T/2$ performed equally well as the up-pumping impeller at $C = T/3$ (see the right panel of Figure 11).

To finish this small exercise in tank-layout variation, the case with $C = T/2$ and a down-pumping impeller was simulated as well; see the right panels of Figure 10. This layout also left some light liquid at the top of the tank for long times. The agitator placed at the same level, $z = H/2$, as the interface very much helped in bringing the mixing time down to levels comparable to those obtained for $C = T/2$ and $C = T/3$ with an up-pumping impeller, as can be witnessed from comparing the data in the two panels in Figure 11.

dx.doi.org/10.1021/ie3000419 | Ind. Eng. Chem. Res. 2012, 51, 6948−6957

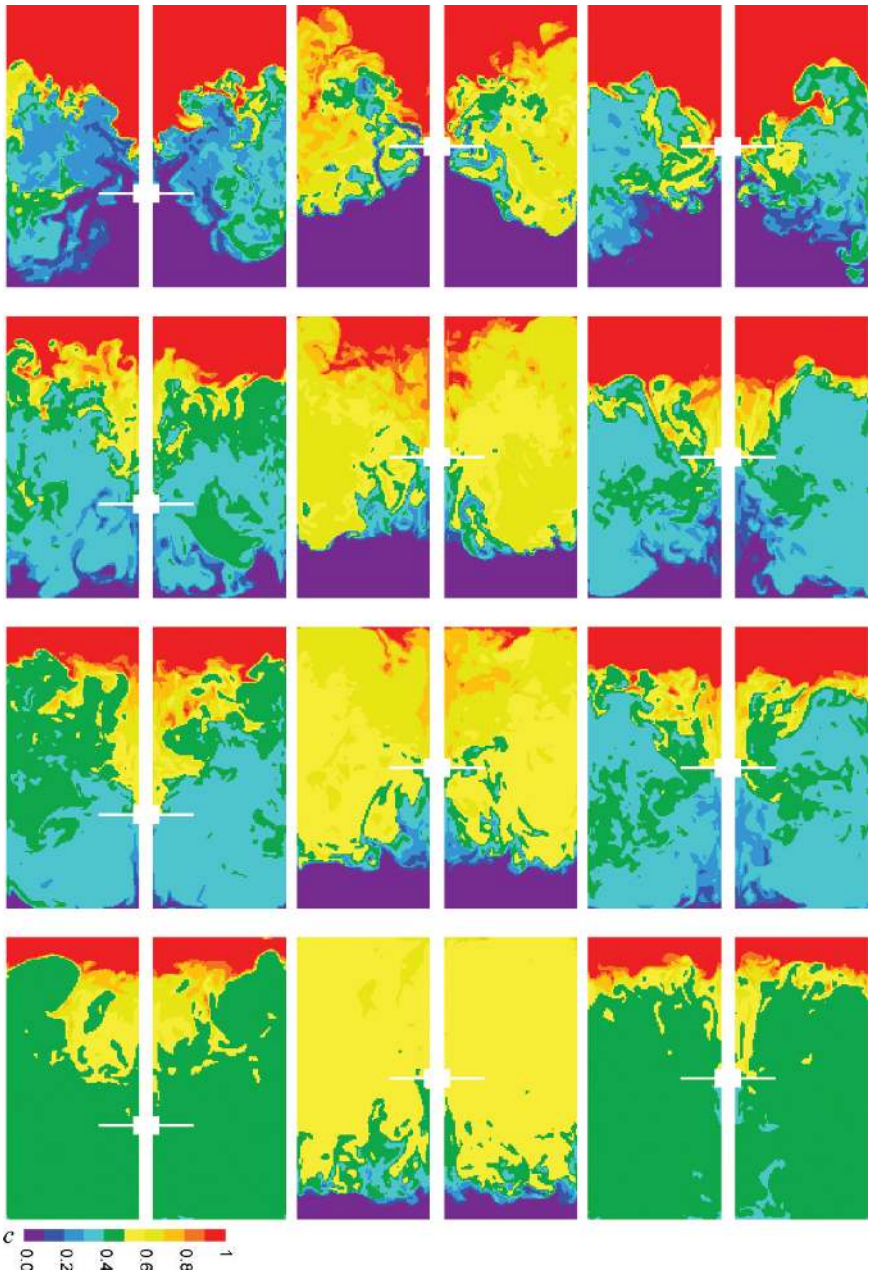

Figure 10. Concentration contours in the midbaffle plane at Re = 6000, Vi = 1, and Ri = 0.5 after (from top to bottom) 10, 20, 30, and 50 impeller revolutions. (Left) Up-pumping impeller at $C = T/3$, (middle) up-pumping impeller at $C = T/2$, and (right) down-pumping impeller at $C = T/2$.

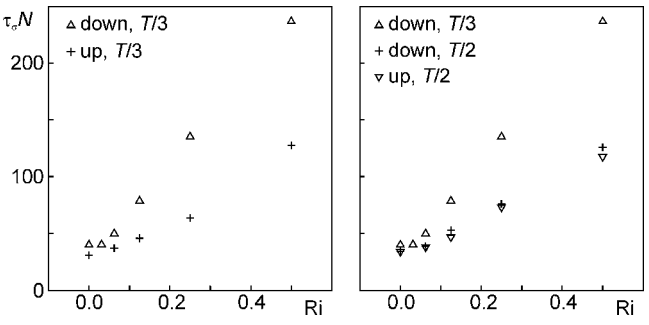

Figure 11. Mixing time based on scalar standard deviation (τ_σ) versus Ri at Re = 6000 and Vi = 1.0. (Left) Comparison between down- and up-pumping impellers at $C = T/3$. (Right) Cases with $C = T/2$ compared with (the default) down-pumping impeller at $C = T/3$.

The results presented so far in this subsection are for Vi = 1.0. As was previously shown in Figure 9 for the default system ($C = T/3$, down-pumping), an increase in viscosity ratio was found to have a minor effect on mixing time for the alternative layouts as well. As an example, we present mixing times for an up-pumping impeller at $C = T/3$ in Figure 12.

Assessment of Resolution Effects. The resolution of the flow dynamics and, even more so, the resolution of the scalar transport were marginal (to say the least) for the default grid with a spacing of $\Delta = T/180$. This resolution was chosen for practical reasons: it allowed us to complete many simulations over many impeller revolutions per simulation. Resolution issues are particularly critical for high Reynolds numbers and also for high viscosity ratios. The former is true because higher Reynolds numbers have a wider spectrum of length scales; the latter because blending a high-viscosity liquid into a low-

dx.doi.org/10.1021/ie3000419 | Ind. Eng. Chem. Res. 2012, 51, 6948−6957

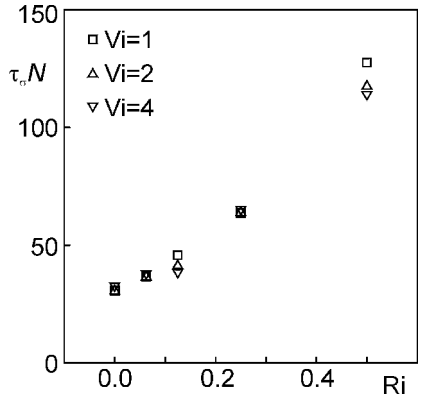

Figure 12. Mixing time based on scalar standard deviation (τ_σ) versus *Ri* at *Re* = 6000 with an up-pumping impeller at $C = T/3$. Comparison between three different viscosity ratios.

viscosity liquid might go through a stage with thin striations of one liquid phase inside the other. Such striations would need to be resolved in a direct simulation. With these points in mind, two cases with the (default) down-pumping impeller at $C = T/3$ were selected for an assessment of grid effects: (1) a case with *Re* = 12000 and further *Ri* = 0.0625 and *Vi* = 1.0 and (2) a case with *Vi* = 4.0, *Re* = 6000, and *Ri* = 0.0. Five grids were compared for case 1, three for case 2. The grids were mainly compared in terms of scalar transport results (concentration fields, decay of scalar variance, and mixing time) because resolution requirements are higher for scalar transport than for flow dynamics and because flow dynamics and scalar transport are tightly coupled: It is not likely that a poor flow field provides a good scalar field.

Figure 13 shows a qualitative comparison of the scalar field for the high-*Re* case on the five grids at the same moment in time (20 revolutions after startup). Although the overall levels of mixing are comparable between the grids, clearly much more detail is captured by the finer grids, with thin structures visible in the impeller outstream for $\Delta = T/552$ that are not there for $\Delta = T/180$. To some extent, this observation is reflected in the decay of scalar variance, as sown in Figure 14. The decays up to $tN \approx 15$ are very similar for the different grids. Beyond 15 revolutions, the decays are slightly slower for the finer grids. This implies that the macroscopic transport is adequately captured by the coarser grid. Once the scalar length scales become finer, diffusion sets in, more quickly so for the coarser grids. At least in terms of the scalar variance, this effect does not lead to very large differences between the grids. The mixing time based on the $\sigma = 0.025$ criterion differs by some 10%, at a maximum, with $\tau_\sigma N$ highest for the finest grid (Figure 14). This 10% we consider (a lower bound for) the accuracy of our mixing time results.

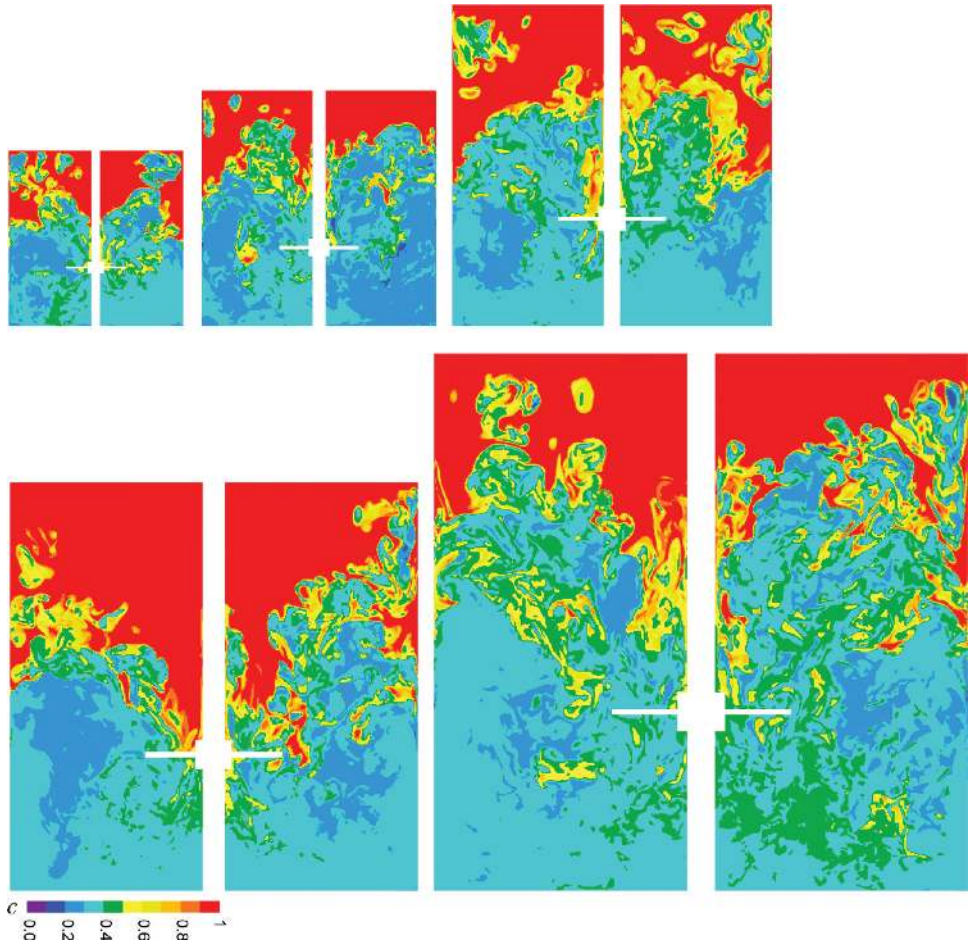

Figure 13. Instantaneous realizations (20 impeller revolutions after startup) of the scalar concentration in the midbaffle plane for *Re* = 12000, *Ri* = 0.0625, *Vi* = 1.0 with a down-pumping impeller at $C = T/3$. Qualitative comparison between different spatial resolutions: $\Delta = T/180$, $\Delta = T/240$, $\Delta = T/330$, $\Delta = T/420$, $\Delta = T/552$. The size of each panel scales linearly with the grid size.

dx.doi.org/10.1021/ie3000419 | *Ind. Eng. Chem. Res.* 2012, 51, 6948–6957

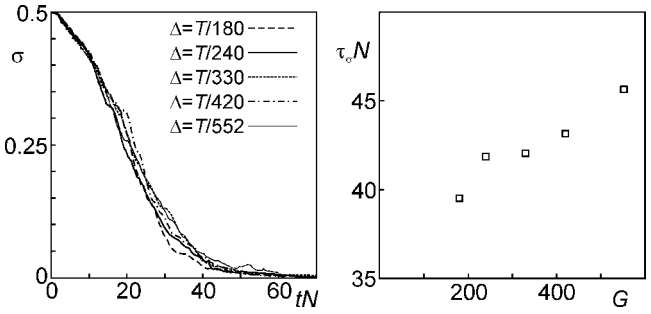

Figure 14. (Left) Scalar standard deviation in the midbaffle plane (σ) as a function of time; comparison at different resolutions for the cases displayed in Figure 13, $\tau_\sigma N$. (Right) Mixing time as a function of resolution, where G is the number of grid spacings per tank diameter T (e.g., for $\Delta = T/180$, $G = 180$).

Grid effects for the high-viscosity-ratio case ($Vi = 4.0$) are presented in a similar fashion in Figure 15. Again, a typical

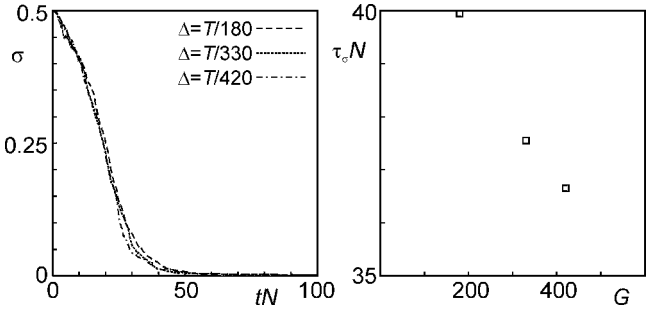

Figure 15. (Left) Scalar standard deviation in the midbaffle plane (σ) as a function of time; comparison at different resolutions for Re = 6000, Ri = 0.0, and Vi = 4.0 for a down-pumping impeller at $C = T/3$. (Right) Mixing time as a function of resolution.

accuracy of 10% can be concluded. The trend in mixing time with respect to resolution is opposite: higher resolution now gives lower $\tau_\sigma N$. Inspection of concentration fields (not shown for brevity) indicates that the entrainment of the low-viscosity liquid in the high-viscosity liquid by the impeller is associated with thin layers of low-viscosity material. These layers are better resolved by the finer grid, (apparently) resulting in faster mixing.

SUMMARY, CONCLUSIONS, AND OUTLOOK

In this work, homogenization of two initially segregated Newtonian liquids with different physical properties (density and viscosity) in stirred tanks was simulated. The tanks were cylindrical, baffled, and flat-bottomed; the impeller was a four-blade, 45° pitched-blade turbine. Given the tank and impeller layout, the blending process is governed by three dimensionless numbers: a Reynolds number (Re), a Richardson number (Ri), and a viscosity ratio (Vi). As a fourth dimensionless parameter, the Schmidt number (Sc), was also identified. It relates to the diffusivity of the two miscible liquids in one another. This diffusivity was assumed to be small, so that Sc was large. In this limit of large Sc, given the resolution limitations of the simulations, it was not possible to investigate the effects of Sc on the blending process.

The Reynolds numbers were in the range of 3000−12000. In this range, indicating transitional and moderately turbulent flow, we did not need to use turbulence modeling to simulate the flow. This was a deliberate choice, as it removes uncertainties as to how the turbulence modeling deals with the local and temporal density and viscosity variations. In our direct simulations, these variations acted on the (resolved) Navier−Stokes equations directly and in a physically consistent manner. At various levels of the simulations, spatial resolution was a concern: (1) Direct simulation of turbulence requires resolution of the flow down to the Kolmogorov length scale. (2) Scalar transport at high Sc values makes the Batchelor scale even smaller. (3) Liquids with different viscosities are known to penetrate one another through thin layers (striations). Resolution was handled in a pragmatic way: through checking the effects of refining the grid on the blending process. The grid spacing was refined up to a factor of 3 from the default grid. In the explicit, three-dimensional simulation procedure based on the lattice-Boltzmann method, such a refinement implies an increase in computational effort of $3^4 = 81$ (the power 4 is the sum of 3 spatial dimensions plus one time dimension). Mixing time variations of 10% between the grids were observed, and the coarsest grid (with 180 grid spacings along the tank diameter) was deemed a fair compromise of accuracy on one side and modest computational demands on the other; it allowed us to run many cases for many impeller revolutions.

With the impeller in down-pumping mode, placed one-third of the tank diameter above the bottom of the tank, and starting from a stable stratification, the Richardson number was found to have the most impact on the blending process: the mixing time steeply increases with increasing Ri. For high Ri (on the order of 0.5), blending is largely due to erosion of the interface between dense liquid and light liquid. Erosion is brought about by the agitation of the denser liquid underneath the interface; the lighter liquid near the top hardly feels the action of the impeller. At the other side of the Ri spectrum, buoyancy effects become insignificant for Ri on the order of 0.03. The increase of mixing time with Ri is more pronounced at lower Reynolds numbers than for higher Re. The viscosity ratio has a weak impact on the mixing time, at least in the viscosity ratio range ($1 \leq Vi \leq 4$) investigated in this work.

Simple geometrical measures can bring down the mixing time significantly: Changing from down- to up-pumping mode decreases the mixing time by a factor of sometimes more than 2. The same holds true for changing the vertical location of the impeller. The key issue in decreasing the mixing time for both design measures is more direct agitation of the interface between the two liquids.

This purely computational study asks for experimental guidance and (possibly/hopefully) validation. Specifically, the numerical issues regarding resolution require experimental assessment. It should be noted, however, that experiments also face resolution questions. For instance, in visualization experiments that would monitor the decay of scalar variance as a metric for mixing (analogously to what we did simulation-wise), the scalar variance is to some extent a function of the resolution and dynamic range of the recording device (i.e., the camera).

AUTHOR INFORMATION

Corresponding Author

*E-mail: jos@ualberta.ca.

Notes

The authors declare no competing financial interest.

dx.doi.org/10.1021/ie3000419 | Ind. Eng. Chem. Res. 2012, 51, 6948−6957

REFERENCES

(1) Derksen, J. J. Blending of miscible liquids with different densities starting from a stratified state. *Comput. Fluids* **2011**, *50*, 35.
(2) Hinze, J. *Turbulence*; McGraw-Hill: New York, 1975.
(3) Lesieur, M.; Metais, O. New trends in large eddy simulation of turbulence. *Annu. Rev. Fluid Mech.* **1996**, *28*, 45.
(4) Hanjalic, K; Launder, B. E. Reynolds stress model of turbulence and its application to thin shear flows. *J. Fluid Mech.* **1972**, *52*, 609.
(5) Bakker, A.; Van den Akker, H. E. A. Single-Phase Flow in Stirred Reactors. *Trans. Inst. Chem. Eng. A* **1994**, *72*, 583.
(6) Eggels, J. G. M. Direct and large-eddy simulations of turbulent fluid flow using the lattice-Boltzmann scheme. *Int. J. Heat Fluid & Flow* **1996**, *17*, 307.
(7) Ng, K.; Fentiman, N. J.; Lee, K. C.; Yianneskis, M. Assessment of sliding mesh CFD predictions and LDA measurements of the flow in a tank stirred by a Rushton impeller. *Trans. Inst. Chem. Eng. A* **1998**, *76*, 737.
(8) Hartmann, H.; Derksen, J. J.; Montavon, C.; Pearson, J.; Hamill, I. S.; Van den Akker, H. E. A. Assessment of large eddy and RANS stirred tank simulations by means of LDA. *Chem. Eng. Sci.* **2004**, *59*, 2419.
(9) Coroneo, M.; Montante, G.; Paglianti, A.; Magelli, F. CFD prediction of fluid flow and mixing in stirred tanks: Numerical issues about the RANS simulations. *Comput. Chem. Eng.* **2011**, *35*, 1959.
(10) Rielly, C. D.; Pandit, A. B. The mixing of Newtonian liquids with large density and viscosity differences in mechanically agitated contactors. In *Proceedings of the 6th European Conference on Mixing, Pavia, Italy*; Springer: New York, 1988; p 69.
(11) Bouwmans, I.; Bakker, A.; Van den Akker, H. E. A. Blending liquids of differing viscosities and densities in stirred vessels. *Chem. Eng. Res. Des.* **1997**, *75*, 777.
(12) Chen, S.; Doolen, G. D. Lattice Boltzmann method for fluid flows. *Annu. Rev. Fluid Mech.* **1998**, *30*, 329.
(13) Succi, S. *The Lattice Boltzmann Equation for Fluid Dynamics and Beyond*; Clarendon Press: Oxford, U.K., 2001.
(14) Frisch, U.; Hasslacher, B.; Pomeau, Y. Lattice-gas automata for the Navier−Stokes equation. *Phys. Rev. Lett.* **1986**, *56*, 1505.
(15) Somers, J. A. Direct simulation of fluid flow with cellular automata and the lattice-Boltzmann equation. *Appl. Sci. Res.* **1993**, *51*, 127.
(16) Goldstein, D.; Handler, R.; Sirovich, L. Modeling a no-slip flow boundary with an external force field. *J. Comput. Phys.* **1993**, *105*, 354.
(17) Derksen, J.; Van den Akker, H. E. A. Large-eddy simulations on the flow driven by a Rushton turbine. *AIChE J.* **1999**, *45*, 209.
(18) Hartmann, H.; Derksen, J. J.; Van den Akker, H. E. A. Mixing times in a turbulent stirred tank by means of LES. *AIChE J.* **2006**, *52*, 3696.
(19) Derksen, J. J. Scalar mixing by granular particles. *AIChE J.* **2008**, *54*, 1741.
(20) Sweby, P. K. High resolution schemes using flux limiters for hyperbolic conservation laws. *SIAM J. Numer. Anal.* **1984**, *21*, 995.
(21) Moin, P.; Mahesh, K. Direct numerical simulation: a tool in turbulence research. *Annu. Rev. Fluid Mech.* **1998**, *30*, 539.
(22) Eswaran, V.; Pope, S. B. An examination of forcing in direct numerical simulations of turbulence. *Comput. Fluids* **1988**, *16*, 257.
(23) Grenville, R. K. Blending of viscous Newtonian and pseudo-plastic fluids. Ph.D. Thesis, Cranfield Institute of Technology, Cranfield, U.K., 1992.
(24) Chapple, D.; Kresta, S. M.; Wall, A.; Afacan, A. The effect of impeller and tank geometry on power number for a pitched blade turbine. *Trans. Inst. Chem. Eng.* **2002**, *80*, 364.